BIO-INSPIRED CATALYSTS FOR THE SOLAR-DRIVEN PRODUCTION OF HYDROGEN GAS

Todd Reynolds, Shinwoo Jeon, Deborah Bebout (advisor), William McNamara (advisor)

College of William & Mary

Abstract

Water splitting through artificial photosynthesis can produce hydrogen gas that can be used as a carbon-free energy source. The reductive half reaction of artificial photosynthesis to generate hydrogen consists of a catalyst, a photosensitizer, and a sacrificial electron donor. Established catalysts for hydrogen evolution utilize expensive metals that hinder industrial scalability of photocatalytic hydrogen evolution. Our group developed three iron and cobalt catalysts capable of generating hydrogen photocatalytically with three distinct sulfur functional groups.

Introduction

Nature is an incredible synthetic and catalytic chemist. Mimicking enzyme active sites with small molecule catalysts has become an important area of research. Successful mimics allow chemists to access reactions that are typically unseen in traditional synthetic methods. One of these reactions is the reduction of acidic protons into hydrogen gas. The ability to produce hydrogen gas with less energetic input would allow hydrogen gas to become a more feasible, carbon-free alternative to fossil fuels. The production of hydrogen gas is a reversible process done by three main enzymes found in green and blue algae; [NiFe] hydrogenase, [FeFe] hydrogenase, and [Fe] hydrogenase.[1] Each active site has cysteine residues paired with small linear molecules with the mononuclear iron active site containing an aromatic nitrogen group.[1] Direct mimics of these active sites have been synthesized and successfully reduce protons, but they suffer from severe degradation over time.[2] Taking the active sites into account, three polypyridyl ligands with sulfur moieties were selected as synthetic targets (Figure 1).
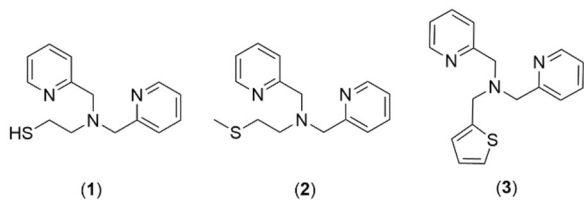

Figure 1. Structures of **1-3**

Polypyridyl rings were chosen for the aromatic nitrogen source due to previous studies in stable, homogeneous proton reducing catalysts.[3] In addition to the cysteine mimic, a methionine mimic and a thiophene mimic were chosen since recent studies have shown that sulfide complexes can produce hydrogen.[4] Herein we report three iron and cobalt catalysts with ligands containing sulfur moieties, that are moderately active for both the photocatalytic and electrocatalytic generation of hydrogen.

Materials and Methods

All experiments were carried out using standard Schlenk techniques under an Ar atmosphere unless otherwise indicated. All reagents were purchased from Acros Organics, Alfa Aesar, Fisher Scientific, or TCI and were used without further purification unless otherwise noted.

Instrumentation

^{1}H and ^{13}C NMR spectra were recorded on an Agilent 400MR DD2 spectrometer operating in the pulse Fourier transform mode. Chemical shifts are reported in ppm and referenced to residual solvent. High-resolution mass spectrometry was conducted using positive-ion mode electrospray ionization with an Apollo II ion source on a Bruker 10 Tesla APEX -Qe FTICR-MS. GC analysis was recorded on a Shimadzu GC-2014 gas chromatograph equipped with a TCD detector, Ar carrier gas, and a packed column.

Data collection, structure solution, and structure refinement of **5**, **6**, **9**, **11**, and **12** were conducted by Todd M. Reynolds at William & Mary. A single crystal was frozen in Parabar oil on a 50 µm Dual-Thickness MicroMount™ and mounted onto a Bruker D8 Venture diffractometer equipped with a PHOTON III photon counting detector. Data collection was carried out using a IµS 3.0 microfocus (Mo) X-ray source. Each structure was solved using SHELXT and refined in SHELXL.[5]

Synthesis of 2-bis(2-methylpyridinyl)amino ethanethiol (**1H**)

Ligand **1H** was synthesized using a modified literature procedure.[6] 2.71 mL of bis(2-methylpyridinyl)amine (BMPA) was added to a 50 mL round bottom flask with 10 mL of toluene under a flow of argon. A condenser and an addition funnel were added on to the round bottom flask under a positive pressure of argon. The BMPA solution was brought to reflux and 1.824 mL of ethylene sulfide was injected into the addition funnel with 10 mL of toluene. Once at reflux, the ethylene sulfide solution was added over 30 minutes and then allowed to reflux for 2 days. The toluene from the yellow solution of **1H** was removed under vacuum. Ligand **1H** was purified in air using a plug of alumina with dichloromethane as the eluent. Once thin layer chromatography showed no trace of **1H**, the dichloromethane in the filtrate was removed under vacuum. The purified yellow oil of **1H** was stored under argon in a refrigerator for future use. (3.11 g, 79.8% yield) ^{1}H NMR (CD$_3$CN, 400 MHz): δ 8.53 (d, 2 H, J = 4.86 Hz), 7.75 (ddd, 2H, J = 1.82, 8.00, 8.00 Hz), 7.59 (d, 2H, J = 7.81 Hz), 7.24 (dd, 2H, J = 2.60, 6.24 Hz), 3.83 (s), 2.78 (m), 2.69 (m). ^{13}C NMR (CD$_3$CN, 400 MHz): δ 159.6, 148.9, 136.3, 123.0, 122.0, 59.8, 56.9, 22.0.

Synthesis of 2-bis(2-methylpyridinyl)aminoethylmethyl sulfide (**2**)

Ligand **2** was synthesized using a modified literature procedure.[7] 5.00 g of sodium bicarbonate was dissolved in 100 mL of dimethylformamide in a 250 round bottom flask under a flow of argon. 2.71 mL of BMPA was injected into the round bottom flask before a condenser was added under a positive pressure of argon. The mixture was brought to reflux and 1.5 mL of 2-chloroethylmethyl sulfide was injected through the condenser. After refluxing overnight, another 1.5 mL of 2-chloroethylmethyl sulfide was injected through the condenser and the mixture was refluxed for 5 days. After 5 days, the solution was cooled to room temperature and vacuum filtered to remove the excess sodium bicarbonate. The filtrate was diluted with 90 mL of dichloromethane and was extracted with 30 mL increments of deionized water until the aqueous layer no longer leeched color. The organic layer was dried with sodium sulfate and minor impurities were removed with an equal amount of decolorizing carbon. The carbon and sodium sulfate were removed from the organic layer with a plug of celite packed with dichloromethane. The dichloromethane was removed from the organic layer under vacuum. Ligand **2** was purified using column chromatography with alumina as the stationary phase and a mix of 3:1 ethyl acetate and hexanes as the eluent. Fractions containing only **2** were combined and the eluent was removed under vacuum. The purified red oil of **2** was stored under argon in a refrigerator for future use. (3.48 g, 84.8% yield) ^{1}H NMR (CD$_3$CN, 400 MHz): δ 8.49 (d, 2 H, J = 4.64 Hz), 7.73 (td, 2H, J = 1.76, 7.72 Hz), 7.59 (d, 2H, J = 7.88 Hz), 7.21 (ddd, 2H, J = 0.60, 4.88, 7.56 Hz), 3.82 (s, 4H), 2.71 (m, 4H), 2.00 (s, 3H). ^{13}C NMR (CD$_3$CN, 400 MHz): δ 159.8, 148.8, 136.3, 122.9, 122.0, 59.9, 53.3, 31.3, 14.6.

Synthesis of bis(2-methylpyridinyl)amino]methyl-2-thiophene (**3**)

Ligand **3** was synthesized using a modified literature procedure.[8] 2.71 mL of BMPA and 2.81 mL of 2-thiophene carboxaldehyde were dissolved in 10 mL of MeOH in a Schlenk tube. 944 mg of sodium

Reynolds

cyanoborohydride dissolved in 10 mL of MeOH was added to the Schlenk tube. Ten drops of glacial acetic acid were added, then the mixture was degassed with argon for 15 minutes. The solution was refluxed for 2 days under 1 atm of argon. The MeOH from the golden-brown solution of **3** was removed under vacuum. Ligand **3** was redissolved in Et_2O and extracted in open air with a saturated aqueous solution of sodium bicarbonate three times. The organic layers were combined and dried with sodium sulfate, which was later removed by gravity filtration. The Et_2O from the organic layers was then removed under vacuum. Ligand **3** was purified using column chromatography with alumina as the stationary phase and a mix of 3:1 ethyl acetate and hexanes as the eluent. Fractions containing only **3** were combined and the eluent was removed under vacuum. The purified dark red oil of **3** was stored under argon in a refrigerator for future use. (2.75 g, 62.0% yield) ^{1}H NMR (CD_3CN, 400 MHz): δ 8.50 (d, 2 H, J = 4.88 Hz), 7.75 (t, 2H, J = 7.64 Hz), 7.63 (d, 2H, J = 7.84 Hz), 7.23 (d, 1H, J = 4.80 Hz), 7.15 (t, 2H, J = 7.80 Hz), 6.94 (d, 2H, J = 5.2 Hz), 3.90 (s, 2H), 3.85 (s, 4H), 2.00 (s, 3H). ^{13}C NMR (CD_3CN, 400 MHz): δ 159.5, 148.8, 136.5, 126.6, 126.2, 125.1, 124.9, 122.7, 122.1, 59.9, 58.7.

Synthesis of Fe(**1**)Cl$_3$ (**4**)

38.2 mg of $FeCl_3*6H_2O$ was dissolved in 4.66 mL of MeCN in a Schlenk tube. The yellow $FeCl_3$ solution was degassed with a flow of argon for 15 minutes, then a balloon filled with argon was added to the tube. 36.6 mg of **1H** and 20 µL TEA was dissolved in 1.00 mL of MeCN that was degassed with argon for 15 minutes. The resulting solution of **1** was injected into the Schlenk tube with an argon-purged needle. The solution was then heated to reflux for 2 hours, during which the solution turned a reddish-brown. Complex **4** was precipitated out of solution using excess TEA and was isolated by vacuum filtration. (49.0 mg, 82.93% yield) The complex was characterized using high-

resolution mass spectrometry. HRMS for $C_{14}H_{16}FeN_3S^+$: predicted m/z= 314.040887, observed m/z= 314.04086.

Synthesis of Fe(**2**)Cl$_3$ (**5**)

36.6 mg of $FeCl_3*6H_2O$ was dissolved in 4.92 mL of MeCN in a Schlenk tube. The yellow FeCl3 solution was degassed with a flow of argon for 15 minutes, then a balloon filled with argon was added to the tube. 37.0 mg of **2** was dissolved in 1.00 mL of MeCN that was degassed with argon for 15 minutes. The resulting solution of **2** was transferred with an argon-purged needle to the $FeCl_3$ solution while stirring. The solution was then heated to reflux for 2 hours, during which the solution turned yellow. Complex **5** was precipitated out of solution using excess Et_2O and was isolated by vacuum filtration. (42.1 mg, 71.35% yield) Yellow plates from dichloromethane and Et_2O. Crystals for structural characterization were made with a slow diffusion of ethyl ether into a highly concentrated solution of **2**. The complex was characterized using x-ray crystallography and high-resolution mass spectrometry. HRMS for $C_{15}H_{19}FeClN_3S^+$: predicted m/z= 364.033215, observed m/z= 364.03323.

Synthesis of Fe(**3**)Cl$_3$ (**6**)

50.3 mg of $FeCl_3*6H_2O$ was dissolved in 6.450 mL of MeCN in a Schlenk tube. The yellow $FeCl_3$ solution was degassed with a flow of argon for 15 minutes, then a balloon filled with argon was added to the tube. 55.1 mg of **3** was dissolved in 1.00 mL MeCN that was degassed with argon for 15 minutes. The resulting solution of **3** was transferred with an argon-purged needle to the $FeCl_3$ solution while stirring. The solution was then heated to reflux for 2 hours, during which the solution turned yellow. Complex **6** was precipitated out of solution using excess Et_2O and was isolated by vacuum filtration. (60.7 mg, 77.18% yield) Yellow blocks from MeCN and toluene. Crystals for structural characterization were made with a slow

Reynolds

diffusion of ethyl ether into a highly concentrated solution of **2**. The complex was characterized using x-ray crystallography and high-resolution mass spectrometry. HRMS for $C_{17}H_{17}FeClN_3S^+$: predicted m/z=386.017564, observed m/z=386.01755.

Synthesis of Co(**1**)Cl$_2$ (**7**)

33.7 mg of CoCl$_2$*6H$_2$O was dissolved in 4.66 mL of MeCN in a Schlenk tube. The blue CoCl$_2$ solution was degassed with a flow of argon for 15 minutes, then a balloon filled with argon was added to the tube. 36.6 mg of **1H** and 20 µL TEA was dissolved in 1.00 mL of MeCN that was degassed with argon for 15 minutes. The resulting solution of **1** was injected into the Schlenk tube with an argon-purged needle. The solution was then heated to reflux for 2 hours, during which the solution turned dark brown. Complex **7** was precipitated out of solution using excess TEA and was isolated by vacuum filtration. (27 mg, 50.92% yield) The complex was characterized using high-resolution mass spectrometry. HRMS for $C_{14}H_{16}CoClN_3S^+$: predicted m/z= 352.007998, observed m/z= 352.00797.

Synthesis of Co(**2**)Cl$_2$ (**8**)

32.2 mg of CoCl$_2$*6H$_2$O was dissolved in 4.92 mL of MeCN in a Schlenk tube. The blue CoCl$_2$ solution was degassed with a flow of argon for 15 minutes, then a balloon filled with argon was added to the tube. 37.0 mg of **2** was dissolved in 1.00 mL of MeCN that was degassed with argon for 15 minutes. The resulting solution of **2** was transferred with an argon-purged needle to the CoCl$_2$ solution while stirring. The solution was then heated to reflux for 2 hours, during which the solution turned dark purple. Complex **8** was precipitated out of solution using excess Et$_2$O and was isolated by vacuum filtration. (22.0 mg, 40.62% yield) Crystals were grown according to literature procedures.[7]

Synthesis of Co(**3**)Cl$_2$ (**9**)

44.3 mg of CoCl$_2$*6H$_2$O was dissolved in 6.450 mL of MeCN in a Schlenk tube. The blue CoCl$_2$ solution was degassed with a flow of argon for 15 minutes, then a balloon filled with argon was added to the tube. 55.1 mg of **3** was dissolved in 1.00 mL of MeCN that was degassed with argon for 15 minutes. The resulting solution of **3** was transferred with an argon-purged needle to the CoCl$_2$ solution while stirring. The solution was then heated to reflux for 2 hours, during which the solution turned dark purple. Complex **9** was precipitated out of solution using excess Et$_2$O and was isolated by vacuum filtration. (36.3 mg 45.73%) Purple blocks from MeOH and Et$_2$O Crystals for structural characterization were made with a slow diffusion of ethyl ether into a highly concentrated solution of **9**. The complex was characterized using x-ray crystallography and high-resolution mass spectrometry. HRMS for $C_{17}H_{17}CoClN_3S^+$: predicted m/z=389.015823, observed m/z=389.01584.

Synthesis of Zn(**1**)Cl$_2$ (**10**)

79.5 mg of **1H** and 20 µL 0.2M NaOH in MeOH was dissolved in 7.75 mL of MeOH in open air. 41.8 mg of ZnCl$_2$ dissolved in 4.50 mL of MeCN was added dropwise to the solution of **1** while stirring. 12.27 mL of toluene was added to the remaining solution to act as an antisolvent. The mixture was then equally divided into four separate vials with loose lids to allow for the slow evaporation of MeOH (103 mg, 84.90% yield). After two weeks, colorless blocks of **10** were harvested from both vials. Crystals were grown according to literature procedures.[9]

Synthesis of Zn(**2**)Cl$_2$ (**11**)

42.4 mg of **2** was dissolved in 3.58 mL of MeCN in open air. 21.2 mg of ZnCl$_2$ dissolved in 2.50 mL of MeCN was added dropwise to the solution of **2** while stirring. 6.08 mL of toluene was added to the remaining solution to act as an antisolvent. The mixture was then equally divided into

Reynolds

two separate vials with loose lids to allow for the slow evaporation of MeCN (50.54 mg, 79.52% yield). After two weeks, colorless blocks of **11** were harvested from both vials. The complex was characterized using x-ray crystallography

Synthesis of Zn(**3**)Cl$_2$ (**12**)

40.9 mg of **3** was dissolved in 2.54 mL of MeCN in open air. 18.9 mg of ZnCl$_2$ dissolved in 2.00 mL of MeCN was added dropwise to the solution of **3** while stirring. 4.94 mL of toluene was added to the solution to act as an antisolvent. The mixture was then equally divided into two separate vials with loose lids to allow for the slow evaporation of MeCN. After three weeks, colorless blocks of **12** were harvested from both vials. (48.4 mg, 81.01% yield) The complex was characterized using x-ray crystallography

Cyclic Voltammetry

All electrochemical experiments were performed under an Ar atmosphere at 23°C and 1 atm using a CH Instruments 620D potentiostat with a CH Instruments 680 amp booster. Cyclic voltammograms (CVs) were taken using a standard three-electrode cell, including a saturated calomel electrode (SCE), platinum auxiliary electrode, and glassy carbon working electrode. The platinum and glassy carbon electrodes were polished prior to each CV using 0.05 µm alumina powder on a cloth-covered polishing pad and rinsed thoroughly with deionized water and acetonitrile. All electrochemical experiments were performed on crystals of each metal complex with recrystallized TBAPF$_6$.

Acid Addition Studies

0.2 g of TBAPF$_6$ (0.1 M), and 0.3 mg of crystalline **1-12** (0.1 mM) were dissolved in 5.0 mL acetonitrile in an electrochemical cell. The resulting solution was degassed with argon for 10 minutes. A background CV scan was obtained with no added acid, then 20 µL of 0.11 M TFA was added for each

subsequent scan. Electrodes were polished between every scan.

Photochemical Hydrogen Evolution

Hydrogen evolution was determined using test tubes with 1:1 ethanol:deionized water solvent, varying amounts of **4-12**, 1.8 mM fluorescein, and 5% triethylamine (TEA, v/v%). Immediately after the addition of TEA, the test tubes were sealed with a septum and copper wire. The test tubes were degassed with argon for 10 minutes in the dark. A Hamilton syringe was used to remove 1.0 mL of argon from the headspace of the test tube and 1.0 mL of methane was added as an internal standard. The test tubes were irradiated with green light (520 nm wavelength) while stirring. After irradiation, 0.10 mL of headspace was removed using a Hamilton gas syringe and injected into a gas chromatograph to determine the ratio of hydrogen to methane to determine hydrogen produced.

Results and Discussion

Since iron polypyridyl complexes with chloro ligands have well known catalytic activity, **1** was complexed with ferric chloride, cobaltous chloride, and zinc chloride.[10] Ligands **2** and **3** coordinated with the iron(III) ion resulted in complexes **5** and **6**, respectively (Figure 3).
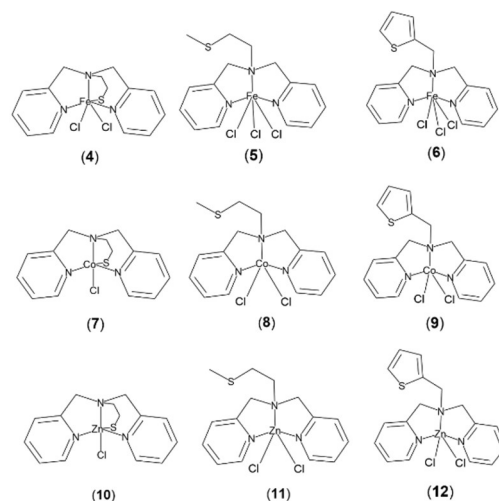

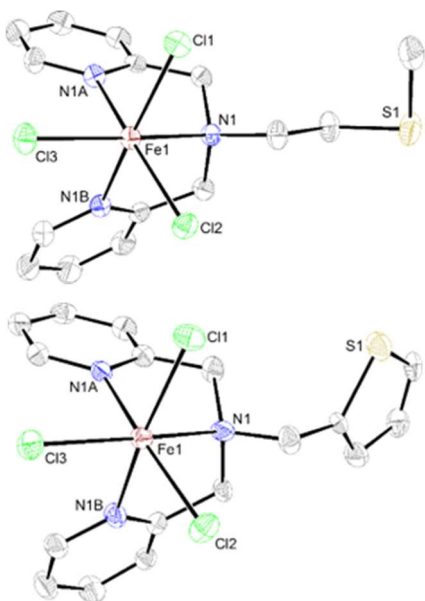**Figure 2.** Structures of **4-12**.

Reynolds

Figure 3. ORTEP Diagrams of **5** (top) and **6** (bottom) with Fe (brown), S (yellow), N (blue), Cl (green), and C (gray). Hydrogen atoms omitted for clarity.

Both structures have a distorted octahedral iron center with a *fac* conformation for the ligand and chlorides. The Fe-N bonds in **5** are 2.185-2.203 Å for the pyridyl rings and 2.287 Å for the tertiary amine. The Fe-Cl bonds in **5** are 2.278-2.292 Å. All N-Fe-N are within 76.57-78.32° and with all other angles within 10% difference of 90° and 180° in **5**. Similarly, the Fe-N bonds in **6** are 2.169-2.206 Å for the pyridyl rings and 2.275 Å for the tertiary amine. The Fe-Cl bonds in **6** are 2.286-2.307 Å. N1-Fe1-N1A and N1-Fe-N1B are 75.69° and 77.09°, respectively, with all other angles within 10% difference of 90° and 180° in **6**. In addition, **6** has a disordered pyridyl ring and thiophene ring position where the ring pivots on the N1-C5 bond and on S1, respectively.

Ligand **3** coordinated with the cobalt(II) ion resulted in complex **9** (Figure 4). Complex **9** has a distorted trigonal bipyramidal cobalt center with a *fac* conformation for the ligand. The Co-N bonds in **9** are 2.071-2.072 Å for the pyridyl rings and 2.315 Å for the tertiary amine. The Co-Cl bonds in **9** are 2.297-2.312 Å. N1-Co1-N1A, N1-Co1-N1B, and Cl1-Co1-Cl2 are 75.36°, 76.00°, and
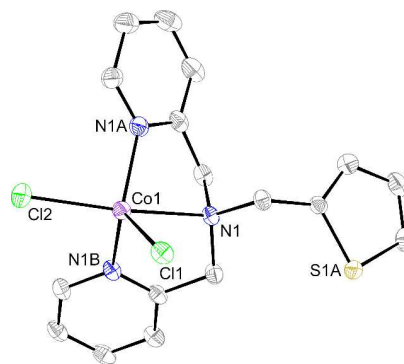

Figure 4. ORTEP Diagram of **9** with Co (purple), S (yellow), N (blue), Cl (green), and C (gray). Hydrogen atoms omitted for clarity.

103.99°, respectively, with all other angles withing 10% difference of 90° and 120° in **9**. In addition, **9** has 180° rotational disorder of the thiophene tail about the C4C-C5C bond.

Ligands **2** and **3** coordinated with the zinc(II) ion resulted in complexes **11** and **12**, respectively (Figure 5). Both structures have a distorted trigonal bipyramidal zinc center with a *fac* conformation for the ligand. The Zn-N bonds in **11** are 2.090-2.101 Å for the pyridyl rings and 2.362 Å for the tertiary amine. The Zn-Cl bonds in **11** are 2.278-2.316 Å. N1-Zn1-N1A, N1-Zn1-N1B, and Cl1-Zn1-Cl2 are 75.34°, 75.23°, and 103.07°, respectively, with all other angles within 10% difference of 90° and 120° in **11**. Similarly, The Zn-N bonds in **12** are 2.169-2.206 Å for the pyridyl rings and 2.275 Å for the tertiary amine. The Zn-Cl bonds in **12** are 2.286-2.307 Å. N1-Zn1-N1A, N1-Zn1-N1B, and Cl1-Zn1-Cl2 are 75.25°, 74.46°, and 105.07°, respectively, with all other angles within 10% difference of 90° and 120° in **12**. In addition, **12** has 180° rotational disorder of the thiophene tail about the C4C-C5C bond.

Surprisingly, none of the complexes with **2** and **3** displayed sulfur-metal bonds, despite the anticipated stability conferred by the chelate effect. Further investigation into the structures reveals close contacts with the sulfide tails of both ligands and π-stacking interactions for the thiophene tail.
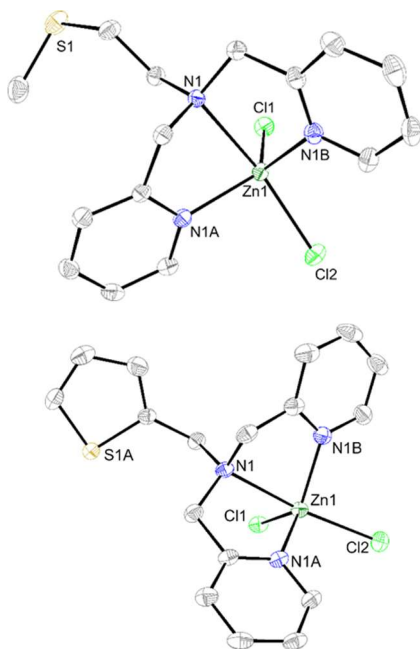
Reynolds

Figure 5. ORTEP Diagrams of **11** (top) and **12** (bottom) with Zn (dark green), S (yellow), N (blue), Cl (green), and C (gray). Hydrogen atoms omitted for clarity.

An irreversible reduction peak with an onset potential of -1.85 V vs. Fc$^+$/Fc was observed in Cyclic Voltammograms of **1-3** upon addition of TFA, which correlates to the protonation of the sulfur atom (Figure 6).
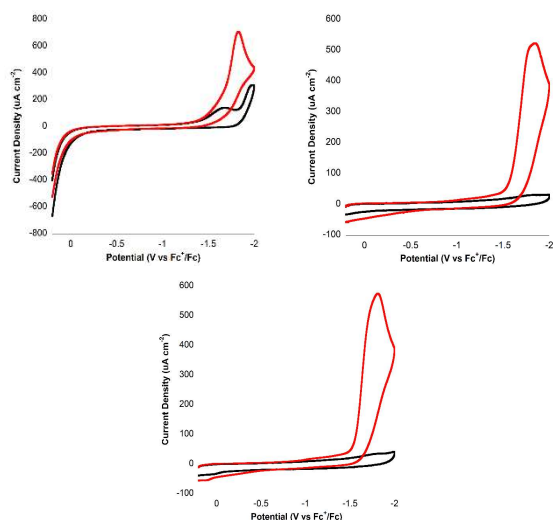
Complexes **4-6** show the Fe(III/II) redox couple at -0.35 V vs. Fc$^+$/Fc. Upon addition of trifluoroacetic acid (TFA), the ligand protonation peak at -1.85 V vs. Fc$^+$/Fc and an additional irreversible reduction peak was observed for each complex that corresponds to catalytic hydrogen generation from acidic protons (Figure 7). The peak observed for complex **4** had an onset potential of -1.55 V vs. Fc$^+$/Fc with an overpotential of 840 mV and an i_c/i_p = 4.86. The peaks observed for **5** and **6** had the same onset potential of -1.60 V vs. Fc$^+$/Fc with an overpotential of 890 mV. Complex **5** had an i_c/i_p = 4.37 and complex **6** had an i_c/i_p = 4.83.

The Co(II/III) redox couple was seen at -0.33 V vs. Fc$^+$/Fc, -1.30 V vs. Fc$^+$/Fc, and -0.90 V vs. Fc$^+$/Fc for complexes **7**, **8**, and **9** respectively. Complexes **7-9** display the ligand protonation peak at -1.85 V vs. Fc$^+$/Fc and an additional irreversible reduction peak with an onset potential of -1.60 V vs. Fc$^+$/Fc with an overpotential of 890 mV upon addition of TFA (Figure 8). Complex **7** had an i_c/i_p = 10.63, complex **8** had an i_c/i_p = 5.19, and complex **9** had an i_c/i_p = 5.65.

Figure 6. CVs of ligands **1** (top left), **2** (top right), and **3** (bottom) with no acid (black), 0.44 mM (blue), 0.88 mM (red), 1.32 mM (yellow) and 1.76 mM (green) TFA.
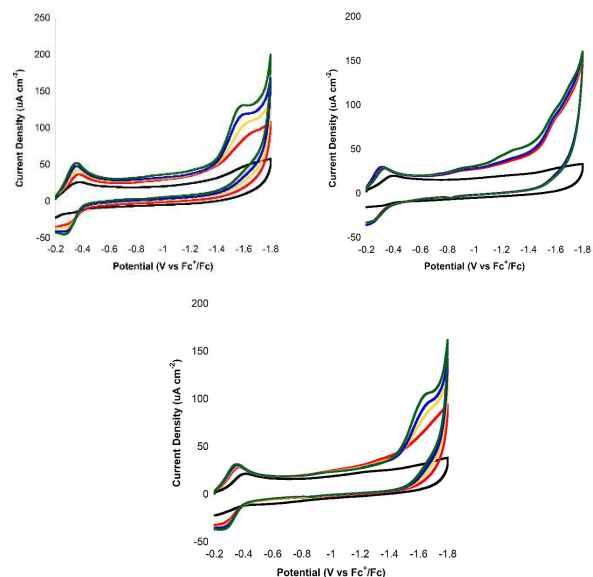

Figure 7. CVs of iron complexes **4** (top left), **5** (top right), and **6** (bottom) with no acid (black), 0.44 mM (blue), 0.88 mM (red), 1.32 mM (yellow) and 1.76 mM (green) TFA.
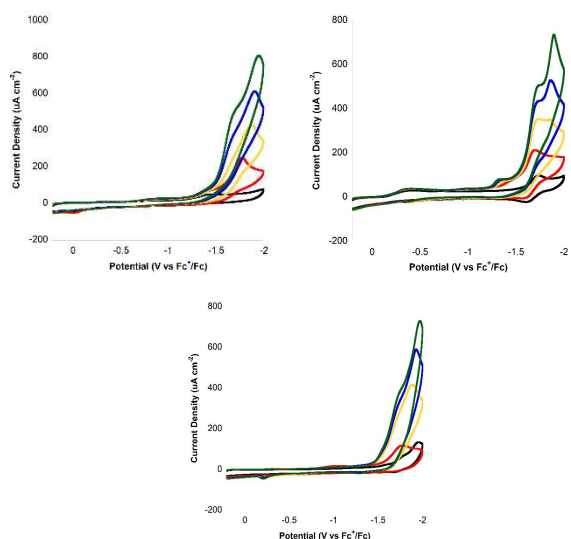
7

Reynolds

Figure 8. CVs of cobalt complexes **7** (top left), **8** (top right), and **9** (bottom) with no acid (black), 0.44 mM (blue), 0.88 mM (red), 1.32 mM (yellow) and 1.76 mM (green) TFA.

Figure 9. CVs of zinc complexes **10** (top left), **11** (top right), and **12** (bottom) with no acid (black), 0.44 mM (blue), 0.88 mM (red), 1.32 mM (yellow) and 1.76 mM (green) TFA.

Since zinc is redox inactive, Cyclic Voltammograms of zinc complexes **10-12** were taken to determine the innocence of each ligand towards catalysis. Complexes **10-12** displayed the peak associated with ligand protonation at -1.85 V vs. Fc^+/Fc upon addition of TFA (Figure 9). In addition, a second peak was observed with an onset potential of -1.6 V vs. Fc^+/Fc upon addition of TFA. The absence of this peak with **1-3** suggests that the peak represents the direct protonation of the zinc center in each complex.

Photocatalysis was used to quantify the amount of hydrogen produced by **4-12**. Upon irradiation with visible light (λ = 520 nm, 0.12 W), hydrogen evolution was observed for solutions containing complexes **4-9**, 1.8 mM of fluorescein, and 5% TEA in a 1:1 water:ethanol mixture. Complexes **4** and **6** had near identical activity with 200 TON after 24 hours (Figure 10). In contrast, complex **5** had lower activity with 25 TON after 24 hours. The sharp decrease in activity for **5** suggests that either an X-type sulfur or an aromatic L-type sulfur is necessary for an efficient
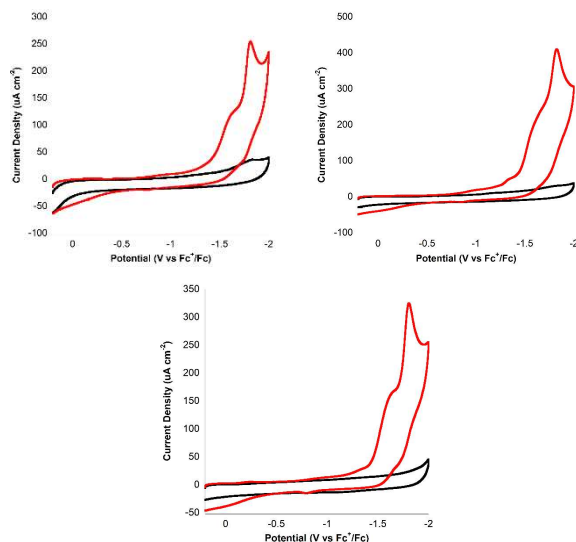
catalytic cycle. It is hypothesized that the stability of an X-type Fe-S bond over an L-type Fe-S bond results in a hydrogen transfer from the thiol to the iron center in **4**. Similarly, it is hypothesized that a hydrogen transfer occurs between the thiophene tail and the iron center in **6** to restore the aromaticity of the thiophene ring. Similar to the iron analogues, complexes **7** and **9** had identical activity with 275 TON after 24 hours (Figure 11). Surprisingly, complex **8** had higher activity with 325 TON after 24 hours. The trend seen in **7-9** is an inversion of the trend seen in **4-6**, as the X-type sulfur and aromatic L-type sulfur reduce the efficiency of the catalytic cycle.

Despite having the same irreversible reduction at -1.6 V vs. Fc^+/Fc as the iron and cobalt analogues, **10-12** displayed no significant hydrogen production (Table 1). Thus, a redox active metal center is required to perform the catalytic cycle, not solely the ligand and metal protonation observed the CVs of the metal complexes.
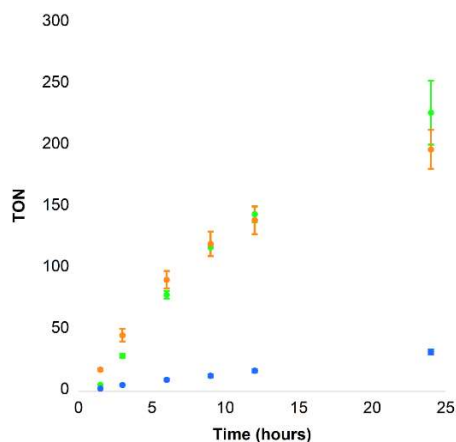
8

Reynolds

Figure 10. Hydrogen generation observed for 25 µM of iron complexes **4** (green), **5** (blue), and **6** (orange) when paired with 1.8 mM Fl and 5% TEA in 1:1 EtOH:Water.
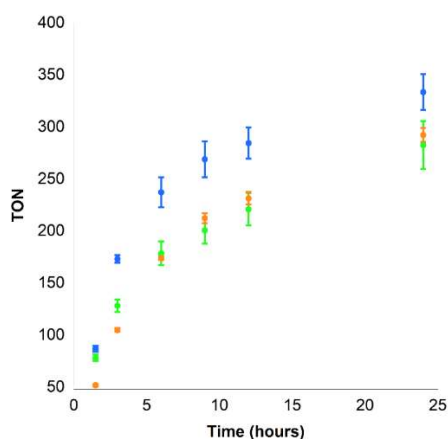

Figure 11. Hydrogen generation observed for 25 µM of cobalt complexes **7** (green), **8** (blue), and **9** (orange) when paired with 1.8 mM Fl and 5% TEA in 1:1 EtOH:Water.

Table 1. TONs of 25 µM **10-12** with 5% TEA in 1:1 ethanol:deionized water after 24 hours

Complex	[Fl] (mM)	H_2 (µL)	TON
10	1.8	Not Observed	0
11	1.8	Not Observed	0
12	1.8	Not Observed	0

Conclusion

In summary, three iron and three cobalt catalyst that mimic hydrogenase were found to generate hydrogen gas at overpotentials of 890-840 mV and i_c/i_p of 4.37-10.63. Zinc analogues, **10-12**, demonstrate that protonation of the ligand and metal can occur under catalytic conditions and may contribute to the catalytic cycle. The photocatalytic activity of **4-9** was tested with fluorescein as a chromophore and TEA as a sacrificial electron donor. Under these conditions, the catalysts exhibited over 200 TON over 24 hours. In addition, the difference in the observed TON for **4-9** suggests that sulfur moieties with highly unfavorable protonation states improve proton reduction with a central iron ion, but hinder proton reduction with a central cobalt ion.

Acknowledgements

9

Reynolds

References

1. Ogo, S.; Kishima, T.; Yatabe, T.; Miyazawa, K.; Yamasaki, R.; Matsumoto, T.; Ando, T.; Kikkawa, M.; Isegawa, M.; Yoon, K.-S.; Hayami, S. *Sci. Adv.* **2020**, *6* (24), eaaz8181. https://doi.org/10.1126/sciadv.aaz8181.

2. Hsieh, C.-H.; Ding, S.; Erdem, Ö. F.; Crouthers, D. J.; Liu, T.; McCrory, C. C. L.; Lubitz, W.; Popescu, C. V.; Reibenspies, J. H.; Hall, M. B.; Darensbourg, M. Y. *Nat Commun* **2014**, *5* (1), 3684. https://doi.org/10.1038/ncomms4684

3. a). Eckenhoff, W. T.; McNamara, W. R.; Du, P.; Eisenberg, R. *Biochimica et Biophysica Acta (BBA) - Bioenergetics* **2013**, *1827* (8–9), 958–973. https://doi.org/10.1016/j.bbabio.2013.05.003. b). Hartley, C. L.; DiRisio, R. J.; Screen, M. E.; Mayer, K. J.; McNamara, W. R. *Inorg. Chem.* **2016**, *55* (17), 8865–8870. https://doi.org/10.1021/acs.inorgchem.6b01413.

4. Reinhard, M. E.; Mara, M. W.; Kroll, T.; Lim, H.; Hadt, R. G.; Alonso-Mori, R.; Chollet, M.; Glownia, J. M.; Nelson, S.; Sokaras, D.; Kunnus, K.; Driel, T. B. V.; Hartsock, R. W.; Kjaer, K. S.; Weninger, C.; Biasin, E.; Gee, L. B.; Hodgson, K. O.; Hedman, B.; Bergmann, U.; Solomon, E. I.; Gaffney, K. J. *Nat Commun* **2021**, *12* (1), 1086. https://doi.org/10.1038/s41467-021-21423-w.

5. Hübschle, C. B.; Sheldrick, G. M.; Dittrich, B. *J Appl Crystallogr* **2011**, *44* (6), 1281–1284. https://doi.org/10.1107/S0021889811043202.

6. Lazarova, N.; Babich, J.; Valliant, J.; Schaffer, P.; James, S.; Zubieta, J. *Inorg. Chem.* **2005**, *44* (19), 6763–6770. https://doi.org/10.1021/ic050735a.

7. Jiang, F.; Siegler, M. A.; Bouwman, E. *Inorganica Chimica Acta* **2019**, *486*, 135–140. https://doi.org/10.1016/j.ica.2018.10.047.

8. Zimmerman, J. R.; De Bettencourt-Dias, A. *Inorganic Chemistry Communications* **2011**, *14* (5), 753–758. https://doi.org/10.1016/j.inoche.2011.02.028.

9. Kurosaki, H.; Tawada, T.; Kawasoe, S.; Ohashi, Y.; Goto, M. *Bioorganic & Medicinal Chemistry Letters* **2000**, *10* (12), 1333–1337. https://doi.org/10.1016/S0960-894X(00)00238-9.

10. Han, Z.; Qiu, F.; Eisenberg, R.; Holland, P. L.; Krauss, T. D. *Science* **2012**, 338 (6112), 1321–1324. https://doi.org/10.1126/science.1227775.
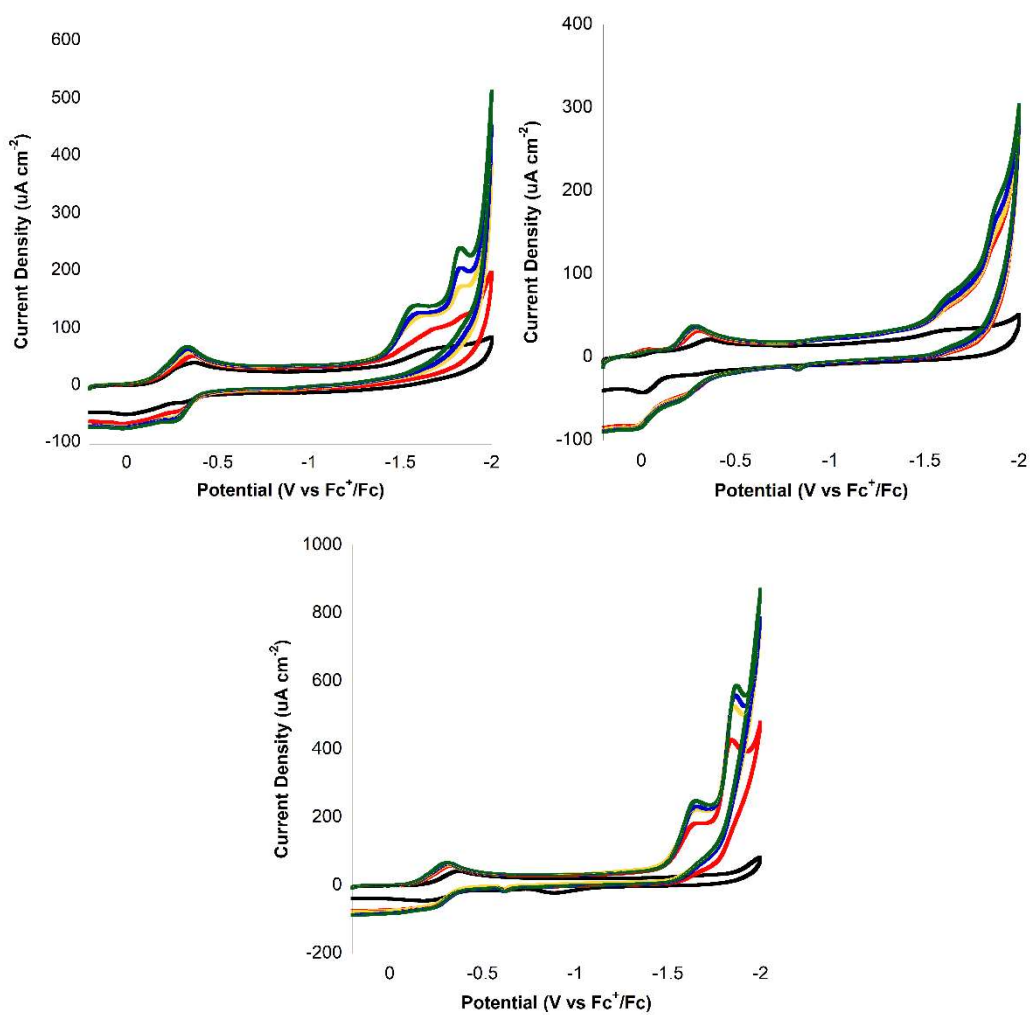
Reynolds

Figure S1. Extended CVs of iron complexes **4** (top left), **5** (top right), and **6** (bottom) with no acid (black), 0.44 mM (blue), 0.88 mM (red), 1.32 mM (yellow) and 1.76 mM (green) TFA. These experiments were performed in MeCN with 0.1M TBAPF$_6$ with scan rate = 200 mV/s.

Reynolds

Figure S2. High resolution mass spectrometry results of **4** (left) and **5** (right). The expected molecular ions were observed with a difference of less than 1 ppm.
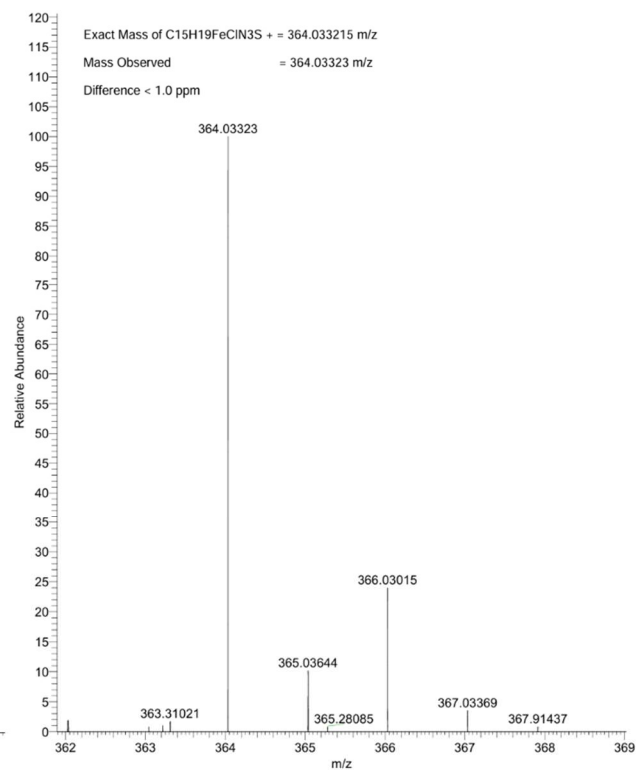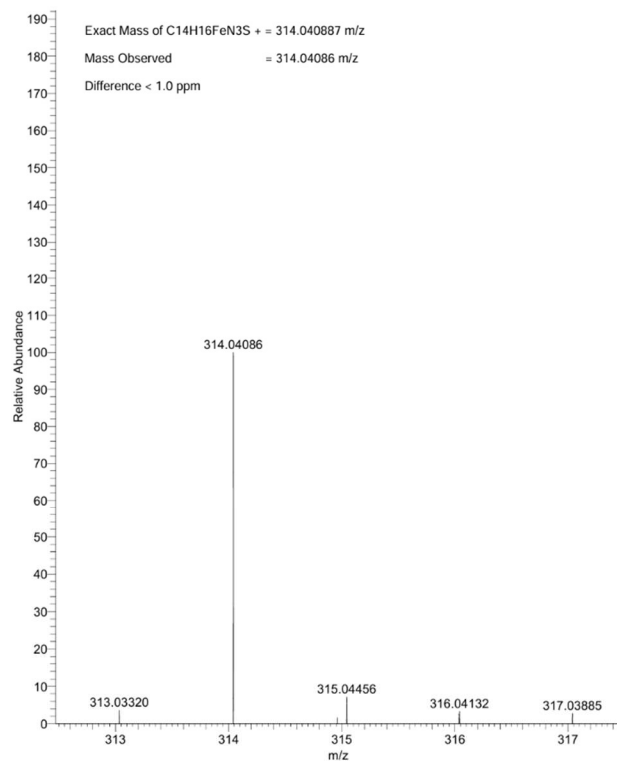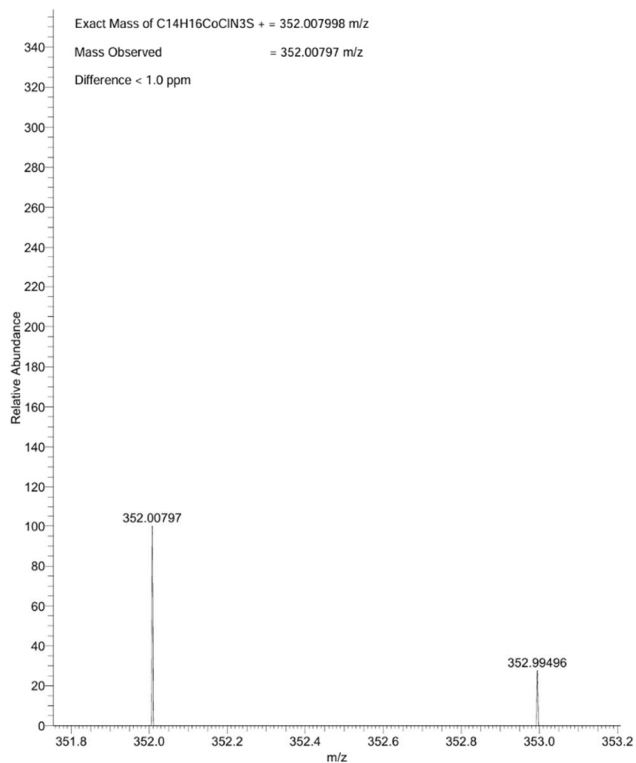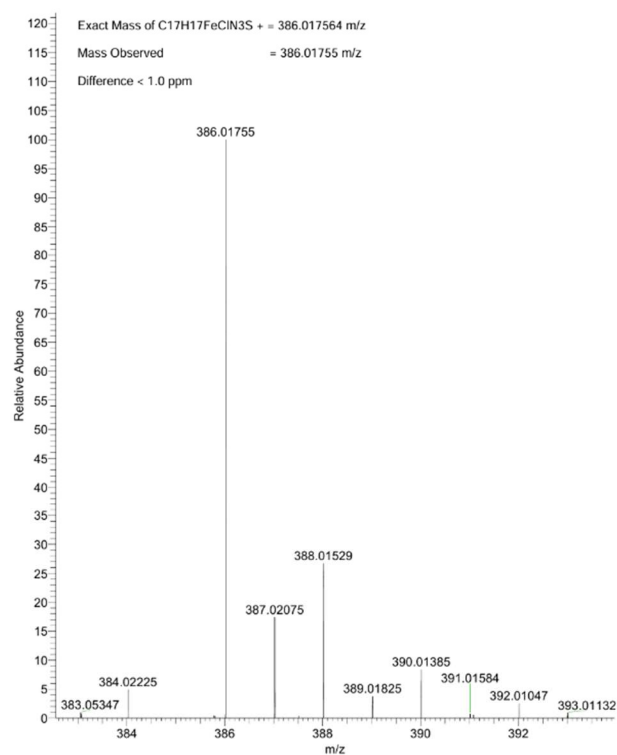

Figure S3. High resolution mass spectrometry results of **6** (left) and **7** (right). The expected molecular ions were observed with a difference of less than 1 ppm.

Reynolds
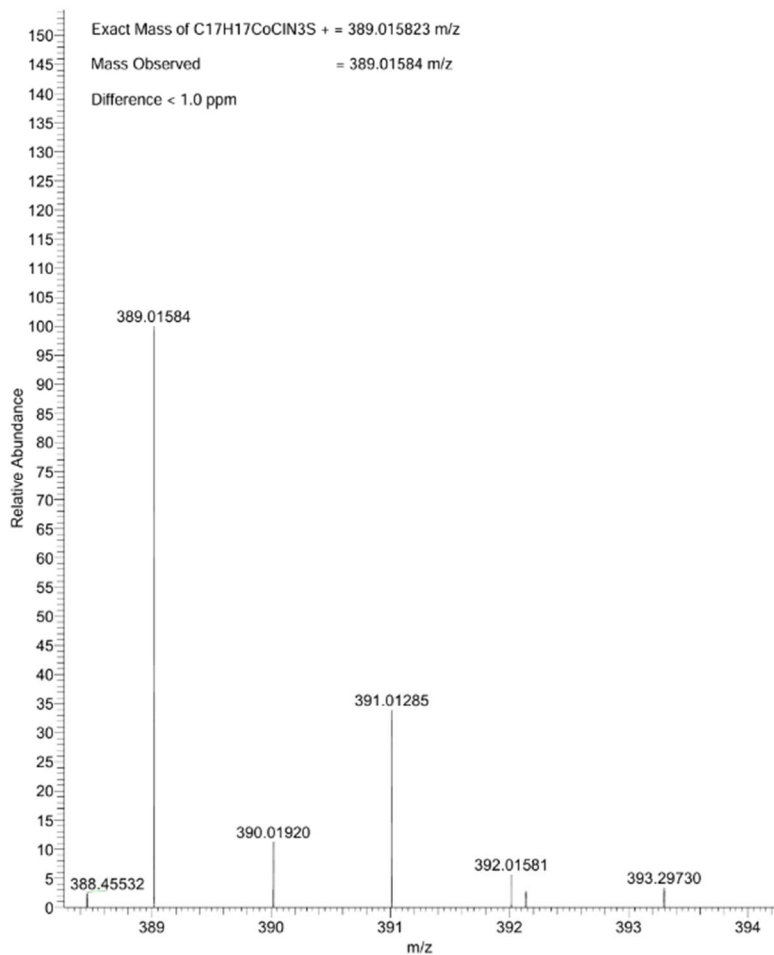
Figure S4. High resolution mass spectrometry results of **9**. The expected molecular ions were observed with a difference of less than 1 ppm.

Table S1. Crystal Data and Refinement Results for **5**, **6**, and **9**

complex	**5**	**6**	**9**
emp. formula	$C_{15}H_{19}Cl_3FeN_3S$	$C_{17}H_{17}Cl_3FeN_3S$	$C_{17}H_{17}CoCl_2N_3S$
formula weight	435.59	457.59	425.22
crystal system	Monoclinic	Triclinic	Monoclinic
space group	$P2_1/n$	$P\bar{1}$	$P2_1/c$
a /Å	8.7627(5)	7.1782(5)	9.9887(13)
b /Å	22.6379(13)	10.7748(7)	15.116(2)
c /Å	9.3095(5)	12.6255(8)	12.6479(17)
α /°	90	77.654(2)	90

Reynolds

β /°	93.482(2)	87.389(2)	110.938(4)
γ /°	90	81.470(2)	90
V /Å^3	1843.31(18)	943.27(11)	1783.6(4)
Z	4	2	4
ρ_{calc} mg/mm^3	1.570	1.611	1.584
$F(000)$	892	466	868
θ range/°	2.369–26.020	1.955–26.047	2.183–26.019
reflns collected	59487	178551	115784
data/restraints/parameters	3616/0/209	3715/30/311	3499/221/236
goodness-of-fit	1.053	1.079	1.049
R_1 ($I > 2\sigma(I)$)	0.0297	0.0277	0.0234
wR_2 ($I > 2\sigma(I)$)	0.0651	0.0711	0.0578

Table S2. Crystal Data and Refinement Results for **11-12**

complex	**11**	**12**
emp. formula	$C_{15}H_{19}Cl_2N_3SZn$	$C_{17}H_{17}Cl_2N_3SZn$
formula weight	409.66	431.66
crystal system	Monoclinic	Monoclinic
space group	Cc	P2$_1$/c
a /Å	11.2551(5)	9.960(2)
b /Å	11.5852(6)	15.276(4)
c /Å	13.7538(6)	12.557(3)
α /°	90	90
β /°	101.658(2)	110.490(8)
γ /°	90	90
V /Å^3	1756.40(14)	1789.7(7)
Z	4	4
ρ_{calc} mg/mm^3	1.549	1.602
$F(000)$	840	880
θ range/°	2.550–26.009	2.183–26.088
reflns collected	77761	116124

Reynolds

data/restraints/parameters	3407/2/200		3535/221/236
goodness-of-fit	1.049		1.040
R_1 ($I > 2\sigma(I)$)	0.0166		0.0255
wR_2 ($I > 2\sigma(I)$)	0.0390		0.0586

Table S3. Selected Bond Lengths and Angles for **5**

Atoms	Length (Å) or Angle (°)	Atoms	Length (Å) or Angle (°)
Fe(1)-N(1A)	2.1851(19)	Cl(1)-Fe(1)-N(1)	89.07(5)
Fe(1)-N(1B)	2.2030(19)	N(1A)-Fe(1)-Cl(2)	89.60(5)
Fe(1)-Cl(1)	2.2778(7)	N(1B)-Fe(1)-Cl(2)	163.87(5)
Fe(1)-N(1)	2.2869(19)	Cl(1)-Fe(1)-Cl(2)	99.74(2)
Fe(1)-Cl(2)	2.2906(6)	N(1)-Fe(1)-Cl(2)	90.49(5)
Fe(1)-Cl(3)	2.2922(7)	N(1A)-Fe(1)-Cl(3)	94.08(5)
N(1A)-Fe(1)-N(1B)	78.32(7)	N(1B)-Fe(1)-Cl(3)	92.57(5)
N(1A)-Fe(1)-Cl(1)	163.73(5)	Cl(1)-Fe(1)-Cl(3)	97.54(2)
N(1B)-Fe(1)-Cl(1)	89.78(5)	N(1)-Fe(1)-Cl(3)	167.31(5)
N(1A)-Fe(1)-N(1)	77.47(7)	Cl(2)-Fe(1)-Cl(3)	98.99(2)
N(1B)-Fe(1)-N(1)	76.57(7)		

Table S4. Selected Bond Lengths and Angles for **6**

Atoms	Length (Å) or Angle (°)	Atoms	Length (Å) or Angle (°)
Fe(1)-N(1B)	2.1693(17)	N(1)-Fe(1)-Cl(1)	164.62(5)
Fe(1)-N(1A)	2.2075(16)	N(1B)-Fe(1)-Cl(2)	86.13(5)
Fe(1)-N(1)	2.2750(17)	N(1A)-Fe(1)-Cl(2)	165.19(5)
Fe(1)-Cl(1)	2.2864(5)	N(1)-Fe(1)-Cl(2)	91.42(5)
Fe(1)-Cl(2)	2.2895(5)	Cl(1)-Fe(1)-Cl(2)	99.58(2)
Fe(1)-Cl(3)	2.3074(6)	N(1B)-Fe(1)-Cl(3)	167.10(5)
N(1B)-Fe(1)-N(1A)	83.92(6)	N(1A)-Fe(1)-Cl(3)	89.67(4)
N(1B)-Fe(1)-N(1)	77.10(6)	N(1)-Fe(1)-Cl(3)	90.49(5)

Reynolds

Atoms	Length (Å) or Angle (°)	Atoms	Length (Å) or Angle (°)
N(1A)-Fe(1)-N(1)	75.70(6)	Cl(1)-Fe(1)-Cl(3)	98.55(2)
N(1B)-Fe(1)-Cl(1)	92.85(5)	Cl(2)-Fe(1)-Cl(3)	97.83(2)
N(1A)-Fe(1)-Cl(1)	91.85(4)		

Table S5. Selected Bond Lengths and Angles for **9**

Atoms	Length (Å) or Angle (°)	Atoms	Length (Å) or Angle (°)
Co(1)-N(1B)	2.0704(13)	N(1B)-Co(1)-Cl(2)	98.27(4)
Co(1)-N(1A)	2.0718(14)	N(1A)-Co(1)-Cl(2)	96.94(4)
Co(1)-Cl(1)	2.2967(5)	Cl(1)-Co(1)-Cl(2)	103.985(17)
Co(1)-Cl(2)	2.3118(5)	N(1B)-Co(1)-N(1)	76.00(5)
Co(1)-N(1)	2.3150(13)	N(1A)-Co(1)-N(1)	75.36(5)
N(1B)-Co(1)-N(1A)	116.54(5)	Cl(1)-Co(1)-N(1)	89.54(3)
N(1B)-Co(1)-Cl(1)	111.82(4)	Cl(2)-Co(1)-N(1)	166.47(3)
N(1A)-Co(1)-Cl(1)	123.18(4)		

Table S6. Selected Bond Lengths and Angles for **11**

Atoms	Length (Å) or Angle (°)	Atoms	Length (Å) or Angle (°)
Zn(1)-N(1A)	2.090(2)	N(1A)-Zn(1)-Cl(2)	94.67(6)
Zn(1)-N(1B)	2.101(2)	N(1B)-Zn(1)-Cl(2)	98.86(6)
Zn(1)-Cl(1)	2.2778(6)	Cl(1)-Zn(1)-Cl(2)	103.06(3)
Zn(1)-Cl(2)	2.3163(7)	N(1A)-Zn(1)-N(1)	75.34(7)
Zn(1)-N(1)	2.362(2)	N(1B)-Zn(1)-N(1)	75.29(8)
N(1A)-Zn(1)-N(1B)	118.94(7)	Cl(1)-Zn(1)-N(1)	93.50(5)
N(1A)-Zn(1)-Cl(1)	118.30(6)	Cl(2)-Zn(1)-N(1)	163.31(6)
N(1B)-Zn(1)-Cl(1)	115.81(6)		

Table S7. Selected Bond Lengths and Angles for **12**

Atoms	Length (Å) or Angle (°)	Atoms	Length (Å) or Angle (°)

Reynolds

Zn(1)-N(1A)	2.0810(16)	N(1A)-Zn(1)-Cl(2)	97.84(5)
Zn(1)-N(1B)	2.0854(17)	N(1B)-Zn(1)-Cl(2)	96.62(4)
Zn(1)-Cl(1)	2.2662(7)	Cl(1)-Zn(1)-Cl(2)	105.07(2)
Zn(1)-Cl(2)	2.3189(7)	N(1A)-Zn(1)-N(1)	75.23(6)
Zn(1)-N(1)	2.3895(16)	N(1B)-Zn(1)-N(1)	74.46(6)
N(1A)-Zn(1)-N(1B)	115.94(6)	Cl(1)-Zn(1)-N(1)	90.77(4)
N(1A)-Zn(1)-Cl(1)	113.98(5)	Cl(2)-Zn(1)-N(1)	164.16(4)
N(1B)-Zn(1)-Cl(1)	121.41(5)		

Reynolds